Chapter 2 Instabilities induced by wide pumping

From the analysis of the iterative map described in Section 1.2.3, we suspected that the dynamical behaviors are cavity-configuration-dependent near some specific resonators. These specific configurations with g_1g_2 parameters equal to 1/2, 1/4, 3/4 correspond to the 1/4, 1/3, 1/6-transverse-mode degeneracies [1], respectively. However, the previous research on the dynamics near the degeneracies showed some conflictive results. Melnikov et al. [2] found that the laser has continuously smooth quasi-periodic threshold throughout the geometrical stable region, except that some singular points corresponding to the transverse mode degeneracy may become chaotic at high-power pumping. On the contrary, Hollinger et al. [3-5] found that in a laser with high-loss cavity and uniform high-power pumping, the laser's output appears to be chaotic at the configurations that have a g_1g_2 parameter equal to 0.4 but to be only quasi-periodic at $g_1g_2 = 0.5$. In the former case, chaotic behavior was considered a condition in which the phase shift between the adjacent transverse modes per round trip is an irrational multiple of π and does not lie close to any rational number with a small denominator. As in the configuration of $g_1g_2 = 0.5$, whose phase shift is a rational multiple of π, the laser output behaves quasi-periodically, even with much higher pumping. This result contradicts the conclusion described in Ref. 2 that the laser behaves chaotically at the transverse mode degenerate configurations.

In this chapter, we focus on the configuration-dependent instabilities around 1/4, 1/3, and 1/6-transverse-mode degenerate configurations and considered only gain saturation as the nonlinear effect when the pump size is larger than the waist of the cold cavity. The Collin integral [6] and the rate equations were used to model the dynamics of a Gaussian end-pumped solid-state laser. Under high Gaussian pumping at the point of degeneration, the laser output cannot lead to chaotic behavior,

unlike the result described by Melnikov et al. [2] but the same as that of Hollinger and Jung [3]. However, the chaotic region is close to the degeneration, a result that is different from the results of Ref. 3 because the phase shift between the adjacent transverse modes in a round trip is close to $2\pi/3$ for the 1/3-degenerate configuration.

2.1 Numerical model

Consider a plano-concave axially pumped solid-state laser shown in Fig. 2.1. The laser contains of a laser crystal with one of its end faces (I) high-reflection coated as the flat mirror and a curved mirror with radius of curvature R separated from it by a distance L. Let the reference plane be the place where the light beam just leaves the laser crystal in the direction of the curved mirror. Under cylindrical symmetry, propagation of the light field toward the curved mirror and back to the flat mirror (end-face I of the crystal) according to the Collin's integral is [6]

$$E^{-}_{m+1}(r) = \frac{2\pi j}{B\lambda}\int \exp(-jk2L)E^{+}_{m}(r')\exp\{-(j\pi/B\lambda)(A\,r'^{2}+D\,r^{2})\}J_{0}(2\pi r'/B\lambda)r'\,dr' \quad ,(2.1)$$

with round trip transmission matrix $\begin{bmatrix} A & B \\ C & D \end{bmatrix}$. Here $E^{+}_{m}(r')$ and $E^{-}_{m+1}(r)$ are the electric fields of the m-th and the (m+1)-th round trips at the planes immediately after and before the gain medium (denoted by the superscripts + and –), where r' and r are the corresponding radial coordinates, λ is the wavelength of laser, and J_0 the Bessel function of zero order. In a thin-slab approximation, we can relate the electric fields E^{+}_{m+1} to E^{-}_{m+1} (after and before the gain medium) in the same round trip as

$$E^{+}_{m+1}(r) = \rho E^{-}_{m+1}(r)\exp(\sigma \Delta N d)\Pi(r/a), \qquad (2.2)$$

where $1-\rho^2$ is the round-trip energy loss, σ is the stimulated-emission cross section, ΔN is the population inversion per unit volume, d is the length of the active medium, and $\Pi(r/a)$ is an aperture function that equals 1 for r less than aperture radius a and

equals 0 otherwise. Furthermore, assuming that the evolution of the population inversion follows the rate equation of a four-level system, we can write the rate equation as

$$\Delta N_{m+1} = \Delta N_m + R_{pm}\Delta t - \gamma \Delta N_m \Delta t - \frac{|E_m|^2}{E_s^{\,2}} \Delta N_m \Delta t \,, \tag{2.3}$$

where R_{pm} is the pumping rate, Δt is the travel time through the gain medium, E_s is the saturation parameter, γ is the spontaneous decay rate, and N_0 is the total density of the active medium. This method was used to model a single-longitudinal multi-transversal high-power solid-state ring laser [3-5] and to analyze the decay rate of standing-wave laser cavities in the linear regime [7]. It was found that a standing-wave resonator can be approximated by a ring resonator if a thin gain medium is placed close to one of the end mirrors [8]. For a continuous Gaussian pump profile $R_{pm} = R_{p0} \exp(-2r^2/w_p^{\,2})$ with constant pumping beam radius w_p throughout the active medium (thin slab), the total pumping rate over the entire active medium is

$$\int_V R_{pm} dV = P_p / h\nu_p \,, \tag{2.4}$$

where P_p is the effective pumping power and $h\nu_p$ is the photon energy of the pumping laser. Because we considered only single-longitudinal-mode dynamics, we have omitted the dispersion of the active medium, so the gain is assumed to be real. Therefore, we have four control parameters: ρ, R, w_p and P_p, which play important roles in the laser system and are investigated in detail as follows.

In an ordinary axially pumped solid-state laser, the round trip propagation time is many orders of magnitude shorter than the spontaneous decay time, especially in a short cavity. As a result, it would take a large number of iterations to arrive at the final state (which may be stable or unstable). To reduce computation time and

because the quasi-periodic bifurcation point is just above the stable continuous-wave solution, we used the scaling method [7] to magnify γ by 10^4 times to determine the bifurcation points. We also checked some important points without scaling that showed no promising change in the quasi-periodic threshold. To reduce the influence of the diffraction loss, we slightly varied R of the curved mirror rather than changing cavity length L to simulate tuning the laser cavity across the point of degeneration.

The parameters of an axially pumped Nd-YVO_4 laser were used: λ = 1.064 μm, $1/\gamma$ = 50 μsec, $\sigma = 25\times10^{-19}$ cm^2, $N_0 = 1.7\times10^{20}$ cm^{-3}, d = 1 mm, a refractive index of 1.96, and L = 6 cm at 808-nm pumping and setting aperture radius a = 1 mm, which is large enough for g_1g_2 = 1/4. In as much as our results are ascribed mainly to the dependence of laser dynamics on configuration as discussed below, we chose the cavity parameter product g_1g_2 = 1-L/R to be 1/2, 1/4 and 3/4 for studying nonlinear dynamics. These configurations correspond to R = 8, 12 and 24 cm, respectively.

In the numerical simulations, we set the initial values of E and ΔN to zero and added to Eq. (2.2) a term that simulates the spontaneous emission whose amplitude is given by the spontaneous decay term in Eq. (2.3) and a phase obtained from a random generator. To implement the Collin integral by the Romberg method, we divided 1-mm aperture into 1024 segments.

2.2 Beam-propagation-dominant dynamics

As expected, when the laser is continuously pumped slightly above the lasing threshold it starts with relaxation oscillation and eventually converges to the cw steady state. Because Δt is 1/30 of the round-trip time T_{cav} under magnification of γ by p times, the actual relaxation oscillation frequency f_r is equal to the numerical

frequency multiplied by $\sqrt{(T_{cav}/\Delta t)/p}$. When one increases the pump power beyond a certain level, bifurcation, or instability threshold, the laser output is no longer stable but becomes multiperiodic. Figure 2.2(a) shows the evolution of the laser pumped with Gaussian pump radius w_p = 330 μm at P_p = 313 mW above the bifurcation 309 mW at the configuration g_1g_2 = 1/2 with ρ = 0.95. Note that cavity beam radius w_0 is ~142 μm and that Ψ, defined as w_p/w_0, equals 2.32. The laser begins with the relaxation oscillation (~6.08 MHz, corresponding to f_r = 333 KHz) followed by a short period of metastable output and finally develops into a flip-flopping steady-state period-2 solution. The corresponding field intensity profile, like the spot size on the flat-mirror end shown in Fig. 2.2(b), also flip-flops to repeat itself after 2 round trips, in contradiction to the regular situation of self-consistentency after only one round trip. This result is equivalent to what is obtained from the stability analysis of a conservative map involving only Gaussian beam propagation, as in Fig. 4(a) of Ref. 9, where the rotation angle in phase space (spanned by spot size w and the curvature $1/R_g$) per round trip equals π for g_1g_2 = 1/2.

Similarly, both of the transverse-mode-degenerate configurations for the 1/3-degenerate configuration at g_1g_2 = 1/4 and the 1/6-degenerate configuration at g_1g_2 = 3/4 belong to the third-order resonance and need 3 round trips to repeat themselves (or period-3 solutions) in phase space [9]. For the configuration slightly tuned away from its corresponding point of degeneration, e.g., at g_1g_2 = 0.25466 or R = 8.05cm, the laser shows non-decaying quasi-periodic oscillation [Fig. 2.3(a) and its inset]. We can see that the laser emission successively circulates in the resonator to form three branches of oscillation with a period of roughly 293 iterations. This is similar to the evolution of spot size in Fig. 1.2(b) of this thesis.

This period can be determined by $2\pi/|\theta - 2\pi/n|$, where θ is the rotation angle in

phase space per round trip [9], $2\pi/n$ is the closest rational fraction rotation angle in phase space, and n=3 in this case. In Fig. 2.3(b), we plot the evolution of three consecutive states 1, 2, and 3, in (w, $1/R_g$) space for the quasi-periodic case. Assume that the initial state is state 1 and that it will evolve in sequence and rotate at an angle θ per iteration (or per round trip). If $\theta/2\pi$ is a rational number, the dynamics is periodic. Contrarily, if $\theta/2\pi$ is irrational, the initial state will never repeat itself but will precede an angle $n(\theta-2\pi/n)$ (or recede for a negative angle) in phase space after n iterations. As a consequence, an arbitrary initial state will nearly return to itself but will precede (or recede) a minimal angle after $T_p = 2\pi/(n|\theta-2\pi/n|)$ iterations. We therefore define the precession frequency f_p as $\frac{c}{2LT_p}$.

The power spectrum [see Fig. 2.3(c)] of Fig. 2.3(a) shows that a low-frequency peak at 25.6 MHz is f_p, which equals to the beat frequency (f_b) of the two nearly degenerate Laguerre-Gauss modes, $LG_{q,0,0}$ and $LG_{q-2,3,0}$. Although there is a lower order $LG_{q-1,1,1}$ mode that degenerates with the fundamental mode, it will not be excited under cylindrical symmetry. The highest peak at 842 MHz results from circulating among those three oscillating branches and returning to the initial branch every three round trips (as the longitudinal mode spacing is 2.5 GHz). This peak is accompanied by a sideband owing to beating with 25.6-MHz peak. We say that the laser is beam-propagation dominant because it behaves as a conservative system governed by Gaussian beam propagation. Therefore, when the laser is axially pumped a bit above the quasi-periodic threshold about the point of degeneration, the laser behaves as if the beam propagation were dominant.

It is interesting to note that the laser output behaves the same as in a lossless optical resonator described by a conservative map. It seems that the laser will become a conservative system, although it does include dissipative elements such as

gain and gaussian (pump) aperture. For low pumping, the Guassian gain profile is a weak Gaussian aperture and provides the damping mechanism; however, because there is already saturated gain above the instability threshold, the effective radius of the aperture increases. As a result, cavity field propagation dominates the laser dynamics and behaves as a conservative system as illustrated in Ref [9].

2.3 Quasi-periodic threshold

2.3.1 "Good cavity"

Here a "good cavity" means that the cavity loss per round trip is < 10% and also that a class-B laser condition [10] rather than a bad-cavity condition that produces Lorenz-Haken instability [10]. Plotted in Fig. 2.4(a) is a three-dimensional bifurcation diagram that shows quasi-periodic instability threshold P_2 at various values of Ψ near $g_1g_2=1/4$ for $\rho = 0.95$. It is obvious that the system has a V-shaped quasi-periodic threshold with a local minimum at the point of degeneration over $1<\Psi\leq 2$. The farther the cavity is tuned away from the degenerate, the higher the quasi-periodic threshold is. This result confirms our previous prediction [9] that the degenerate configuration is unstable under the nonlinear effect. Moreover, the V-shaped threshold is deeper as Ψ is close to 1 and becomes flat for large Ψ. This shows that the quasi-periodic threshold is independent of cavity configuration if a uniform pump is used, as reported in Ref. 11. Similar results can be obtained with other degenerate configurations.

Fixing $g_1g_2=1/4$, we plotted the ratio (P_2/P_1) of quasi-periodic threshold P_2 to lasing threshold P_1 versus Ψ [Fig. 2.4(b)]. The ratio approaches 1 with uniform pumping for Ψ approaching infinity, and it increases sharply as Ψ becomes close to 1. The result is the same as that derived by Lugiato et al., namely, that instability in terms of the threshold ratio favors a cavity operated with large Ψ, where it is easier to

excite multitransverse modes to develop spatiotemporal instabilities. However, as the lasing threshold increases monotonically as a function of Ψ, a minimal quasi-periodic threshold power of 175 mW occurs at $\Psi \approx 2.3$, where $P_2/P_1 \approx 1.8$. Furthermore, the lasing threshold is almost independent of g_1g_2 about the point of degeneration as $\Psi > 1$; thus the lowest quasi-periodic threshold at the degeneration that is due to sensitivity to nonlinear effects is demonstrated in Ref. (9).

2.3.2 High-loss cavities

We have discussed cavity-configuration-dependent laser dynamics under the good-cavity condition with $\rho = 0.95$. To examine the influence of cavity loss on laser dynamics, we have chosen values of ρ of 0.95, 0.9, 0.8 and 0.7 for $\Psi = 1.3$. From Fig. 2.4(c) we found that the V-shaped threshold behavior disappears as ρ decreases to 0.7. It develops into a monotonically increasing smooth curve with respect to g_1g_2, and the threshold at degeneration is no longer a local minimum. This smooth curve is similar to that described in Ref. 2 for 50% mirror reflection or $\rho^2 = 0.5$. As mentioned above, the laser with high mirror reflectivity mimics a conservative system and becomes propagation dominant when it is operated in a quasi-periodic state. Thus, the V-shaped quasi-periodic threshold will not be found in the research reported in Ref. 2, where a high-loss cavity was considered, nor in Ref. 12, with uniform pumping. Note that these curves are asymmetric. Normally, if the aperture radius and the cavity length are both constant, the larger the g_1g_2 parameter, the larger the spot size is on the flat mirror, which is also a gain medium. Because diffraction loss is minimized by choice of a sufficiently large aperture, in our simulation the asymmetry is ascribed mainly to a change in the overlap integral of the cavity field with the pumping as g_1g_2 varies.

2.4 Bifurcation diagram

It is worth noting that when the laser is pumped just above the bifurcation, the stripe denoted for quasi-period oscillation in Fig. 2.3(a) has less than a 1% variation. Raising the pump power makes the stripe wider. When the pump power is further increased, the laser is operated far away from the linear regime, and its highly saturated gain may cause serious instabilities. Because the instabilities induced by higher pumping may depend on the spontaneous decay rate, we magnify γ only 10 times to investigate the high-pumping condition. In fact, there are minor differences compared with scaling γ by 10 times and 100 times if we simply want to classify the types of instability.

Under a spatially inhomogeneous pump, because of competition between two transverse modes a laser can produce chaotic emission [13]. Thus we suspect that it might be easier to obtain chaos at a minimal quasi-periodic threshold where $\Psi = 2.32$. Indeed, we tried the pump power up to 7 P_1 at $\Psi = 2.32$, but chaos was not found. By using $\Psi = 2.78$, we can classify many kinds of instabilities shown in Fig. 2.5(a) for $\rho = 0.95$. For instance, we defined the so-called modulated quasi-periodic state shown in Fig. 2.5(b) for R = 8.0075cm and $P_p = 400$ mW. Further increasing the pump power, we found so-called modulated pulsing and chaos when R = 8.0075 cm as shown in Fig. 2.5(c) and 2-5(d) for $P_p = 500$ and 600 mW, respectively. In the region where R > 8.015 cm, the laser is in the so-called precession oscillation state, showing three overlapped sinusoidal-like oscillations, as illustrated in Fig. 2.6(a) for R = 8.05 cm and $P_p = 650$ mW. Its corresponding power spectrum is shown in Fig. 2.6(b). We can see that the power spectrum has a precession frequency of 24.75 MHz that is close to 25.6 MHz for lower pumping as in Fig. 2.3(c). The precession oscillation appears to be soft in amplitude and hard in frequency, even for P_p as much as 1 Watt. The inset in Fig. 2.6(b) is the expansion of high-frequency spectrum. The main peak

at 841.6 MHz again corresponds to one third of the longitudinal mode spacing, and the peak at 816 MHz, which has down-shifted ~25 MHz, corresponds to f_p. The presence of small peak, located 150±25 KHz beside the main peaks, is ascribed to beating with the subharmonics of the relaxation oscillation. Note that the numerical relaxation oscillation frequency is now ~350 kHz.

We have plotted in Fig. 2.7(a) the frequencies of the spectral peaks as P_p increases for R = 8.05 cm. At low pump, we had only two peaks, separated by f_p, until P_p = 400 mW, a sideband attributed to frequency beating with relaxation oscillation, appears in the high-frequency region. To show how the spectrum develops as P_p increases, we used a filled circle bisected by a short line to mark the highest peak in that group of spectral peaks. We found not only that the precession frequency is slightly redshifted but also that the subharmonic of the relaxation oscillation appears as increasing P_p; for instance, the frequency spacing of the main peak and its side band at P_p = 600 mW is half that at P_p = 500 mW. Figure 2.7(b) shows the bifurcation diagram for R = 8.0075cm, which is closer to the 1/3-degenerate configuration. As P_p = 350 - 400 mW, the difference between the two peaks near 834 MHz approaches the third harmonic of the relaxation oscillation frequency. Each of the three main peaks shows sideband frequencies due to beating with the relaxation oscillation at P_p = 450 mW. Further increasing the pumping, we observed increasingly more sidebands caused by beating with the subharmonics of the relaxation oscillation; finally the laser became chaos. We believe that either increasing the pumping or tuning the cavity configuration toward the point of degenerates will enhance the gain dynamic effect that will cause subharmonic bifurcation owing to nonlinear gain. A transition from a mechanism that is dominated by beam propagation to one dominated by gain dynamics will result. We can also suppress the diffraction effect by reducing the reflectance; for example, when

ρ = 0.8, the region of chaos becomes wider and farther away from degeneration than for ρ = 0.95.

2.5 Interplay of beam propagation and gain dynamic bifurcation

If we maintain proper pump power and scan over the whole range of R in Fig. 2.5(a) we will obtain instabilities similar to those described in Ref. 12 in which the transverse mode spacing varies about $g_1g_2 = 1$. We can also achieve the results of Fig. 2.5(a) by using Fig. 6 of Ref. 14 where chaos exists within small ranges of phase difference (corresponds to R in our case) and round trip loss (or $1-\rho^2$).

Maintaining P_p at 650 mW, we show in Fig. 2.8 the transverse beat frequency (f_b) of the cold cavity and the precession frequency (f_p) relative to R for ρ = 0.95. We have found that the numerical precession frequency nearly equals the transverse beat frequency when the laser is propagation dominant as $R \geq 8.03$ cm. Another evidence that the propagation-dominant instability surely governed by the diffraction integral is that the precession frequency is independent of the spontaneous-emission rate or gain. As R is tuned toward the degenerate or the chaotic region, however, precession frequency f_p deviates from the transverse beat frequency because the gain dynamics, via the rate equations, begin to play a crucial role in change of the precession frequency. The gain aperture and saturation effects take control of the dynamics when the precession frequency declines to several times the relaxation oscillation frequency as $R \approx 8.01$ cm. In Fig. 2.7(b), for small P_p, two frequencies, ~834 and ~831 MHz, appear to be quasi-periodic, mainly because of beam propagation or diffraction, so their difference is understood as $f_{p.}$ The laser has increasingly sideband frequencies as a result of period multiplication owing to the nonlinear gain through the rate equations for larger P_p. It seems that the route to chaos close to degeneration is the interplay (or the mixing effect) of the quasi-period and the period

multiplied as shown in Fig. 2.7(b).

We believe that the cavity loss $1-\rho^2$ is the key factor that differentiates the results of Melnikov et al. and Hollinger et al. from ours. The V-shaped threshold becomes as smooth as Melnikov's result [Fig. 2.4(c)] for a high-loss cavity. Hollinger et al. obtained their results with a high-loss cavity, but they didn't investigate how close g_1g_2 should be to 0.5 for the laser output to be quasi-periodic but not to become chaotic, [3] however, in our good cavity case the chaotic region becomes narrower and can be close to the degeneracy.

References

[1] A.E. Siegman, Lasers (University Science, Mill Valley, CA), p. 761 (1986).

[2] L. A. Melnikov, S. A. Tatarkova, and G. N. Tatarkov, J. Opt. Soc. Am. B 7, 1286 (1990).

[3] F. Hollinger and Chr. Jung, J. Opt. Soc. Am. B 2, 218 (1985).

[4] R. Hauck, F. Hollinger, and H. Weber, Opt. Commun. 47, 141 (1983).

[5] F. Hollinger, Chr. Jung, and H. Weber, Opt. Commun. 75, 84 (1990).

[6] S.A. Collins, J. Opt. Soc. Am. 60, 1168 (1970).

[7] Y.J. Cheng, P.L. Mussche, and A.E. Siegman, IEEE J. Quantum Electron. 31, 391 (1995).

[8] M. Moller, L. M. Hoffer, G.L. Lippi, T. Ackemann, A. Gahl, and W. Lange, J. Mod. Opt. 45, 1913 (1998).

[9] M.D. Wei, W.F. Hsieh, and C.C. Sung, Opt. Commun. 146, 201 (1998).

[10] C.O. Weiss and R. Vilaseca, Dynamics of Lasers (Weinheim, New York), p. 14, p. 26 (1991).

[11] L. A. Lugiato, F. Prati, L. M. Narducci, P. Ru, J. R. Tredicce and D. K. Bandy, Phys. Rev. A 37, 3847 (1988).

[12] L.A. Lugiato, G.L. Oppo, J.R. Tredicce, L.M. Narducci, and M.A. Pernigo, J. Opt. Soc. Am. B 7, 1019 (1990).

[13] M.L. Shih and P.W. Milonni, Opt. Commun. 49, 155 (1984).

[14] F. Hollinger, Chr. Jung, and H. Weber, J. Opt. Soc. Am. B 7, 1013 (1990).

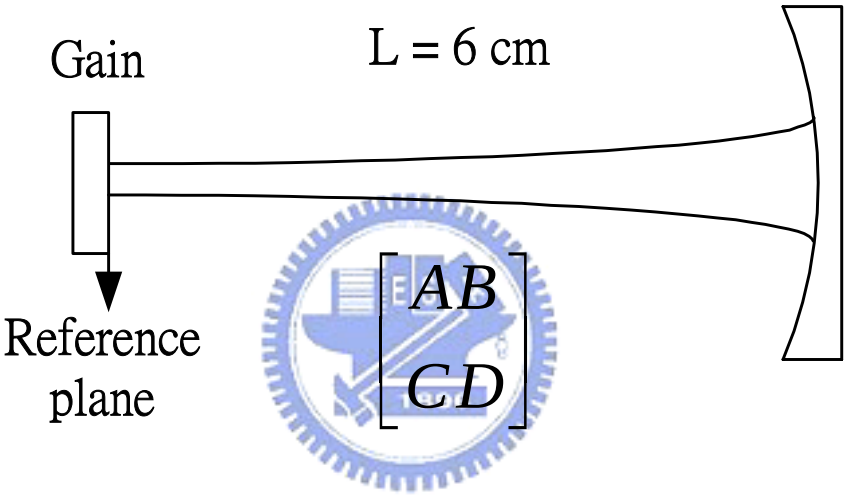

Fig. 2.1. The laser configuration.

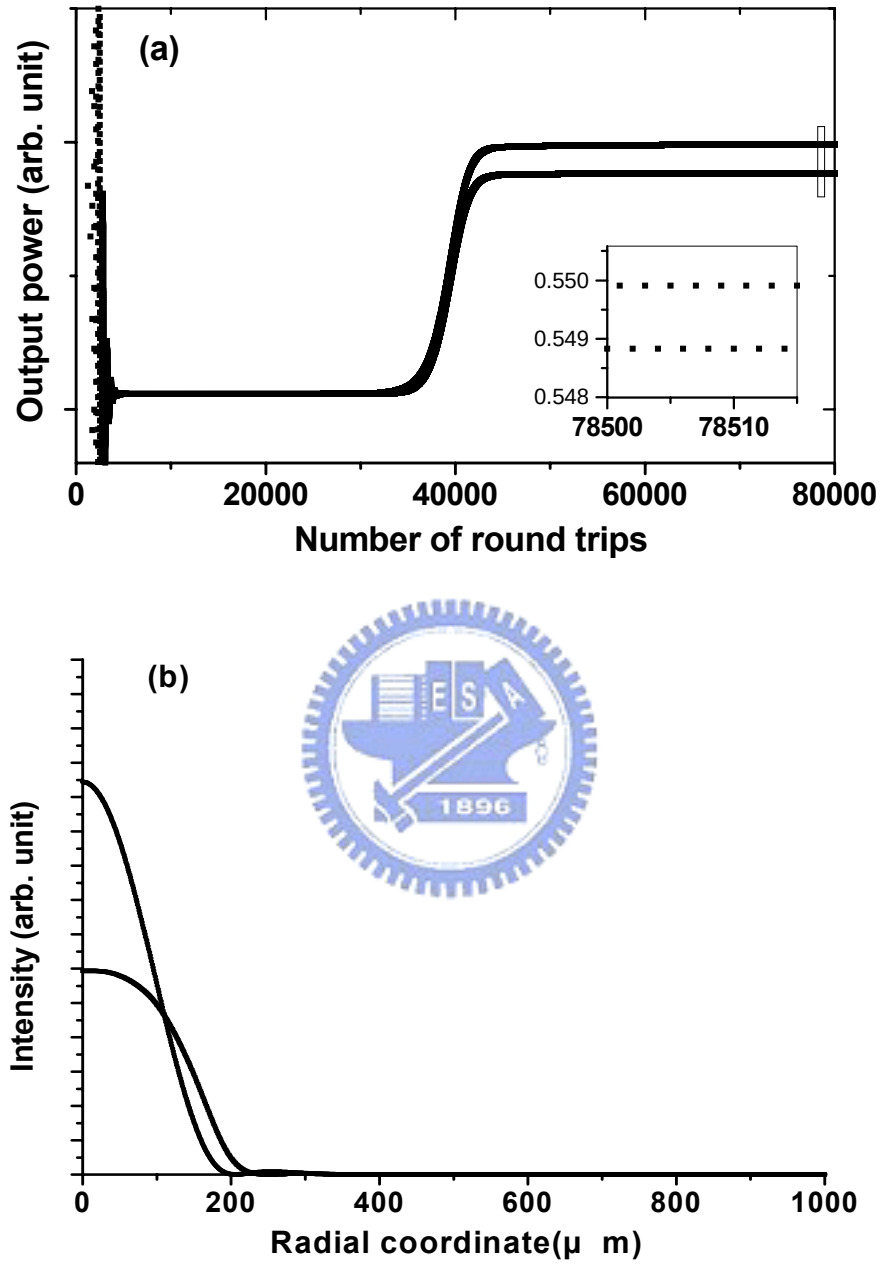

Fig. 2.2. Output power evolution (a) and beam profile (b) of the period-2 steady state for $g_1g_2 = 1/2$ with $\rho = 0.95$ above the instability threshold.

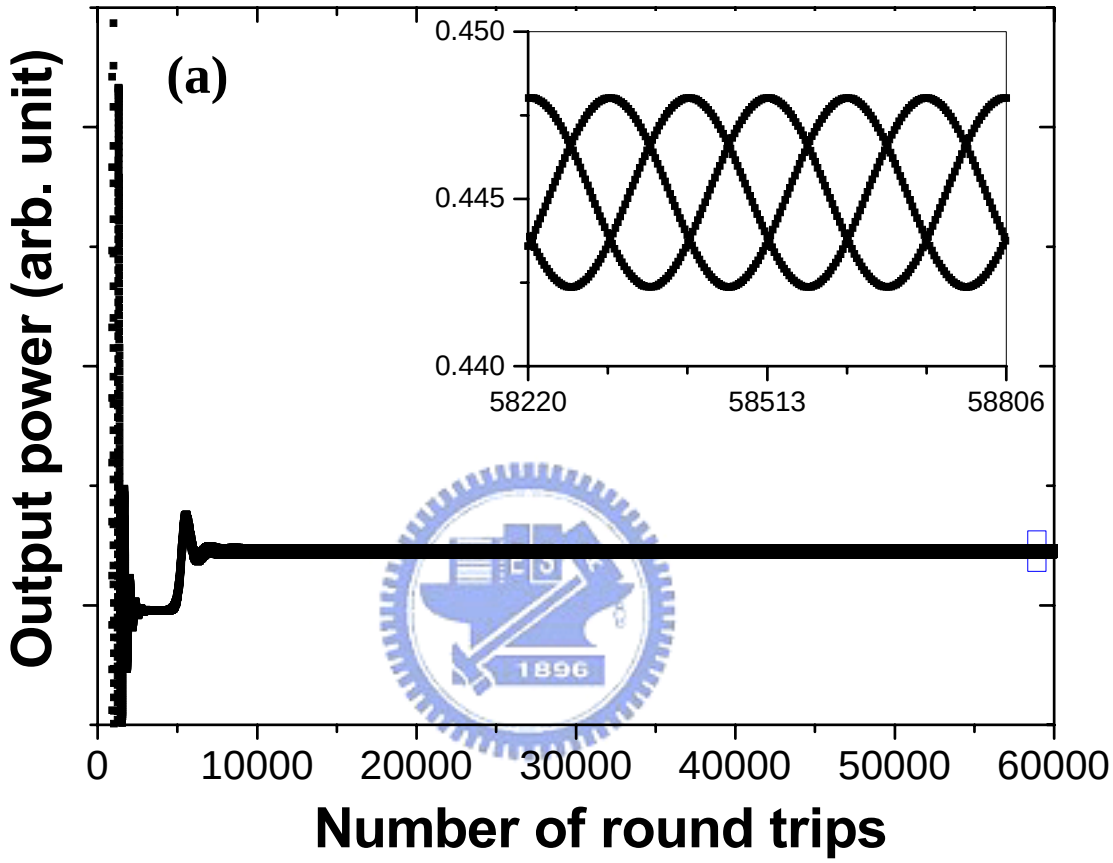

Fig. 2.3. (a) Evolution of the output power of the quasi-periodic oscillation at g_1g_2 = 0.25466, ρ = 0.95, Ψ = 2.32, and P_p = 210mW. Inset (a) is the magnification of six precession periods.

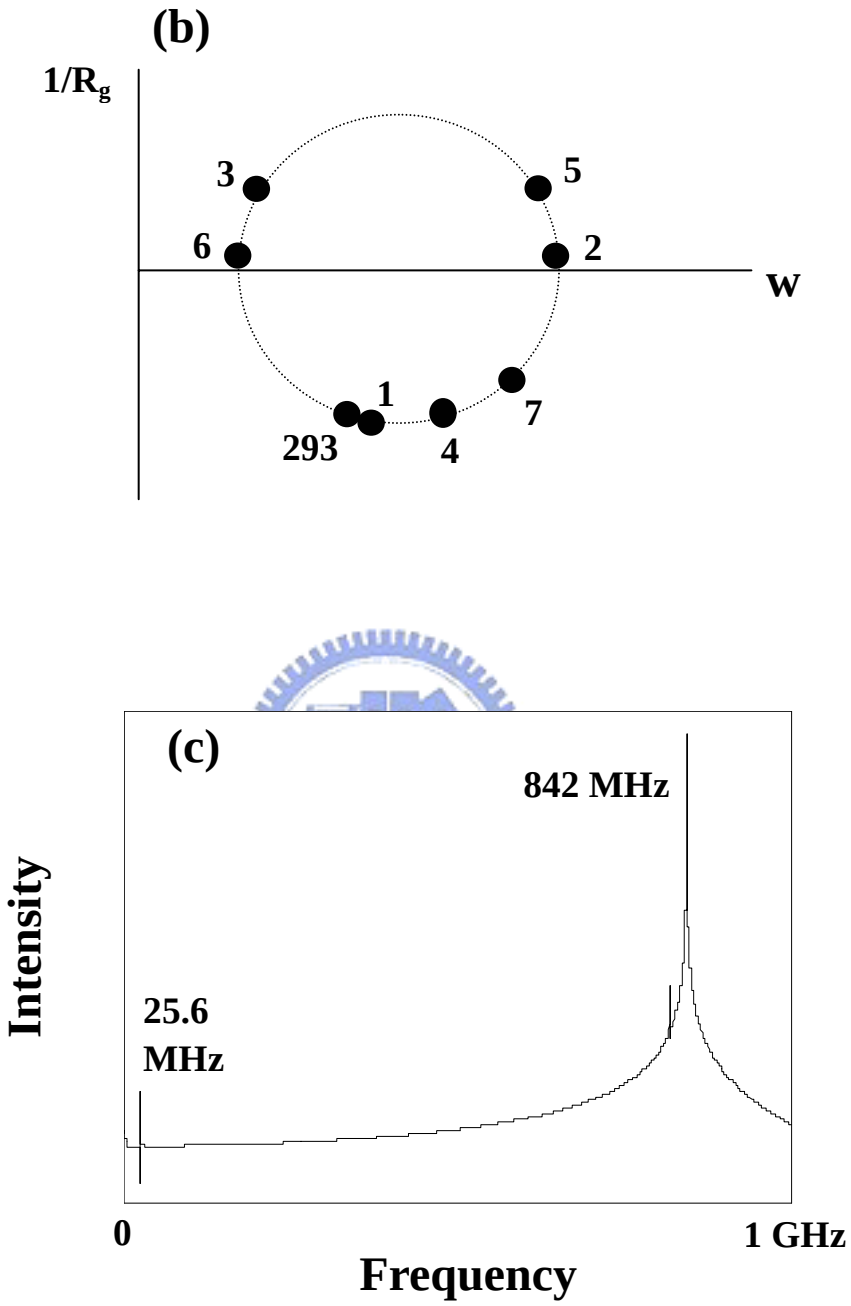

Fig. 2.3. (b) The spot size evolution in (w, $1/R_g$) phase space as in Ref. (9). The precession explains the output power evolution (a) and the power spectrum (c) of the quasi-periodic oscillation for $g_1g_2 = 0.25466$, $\rho = 0.95$, $\Psi = 2.32$, and $P_p = 210$mW.

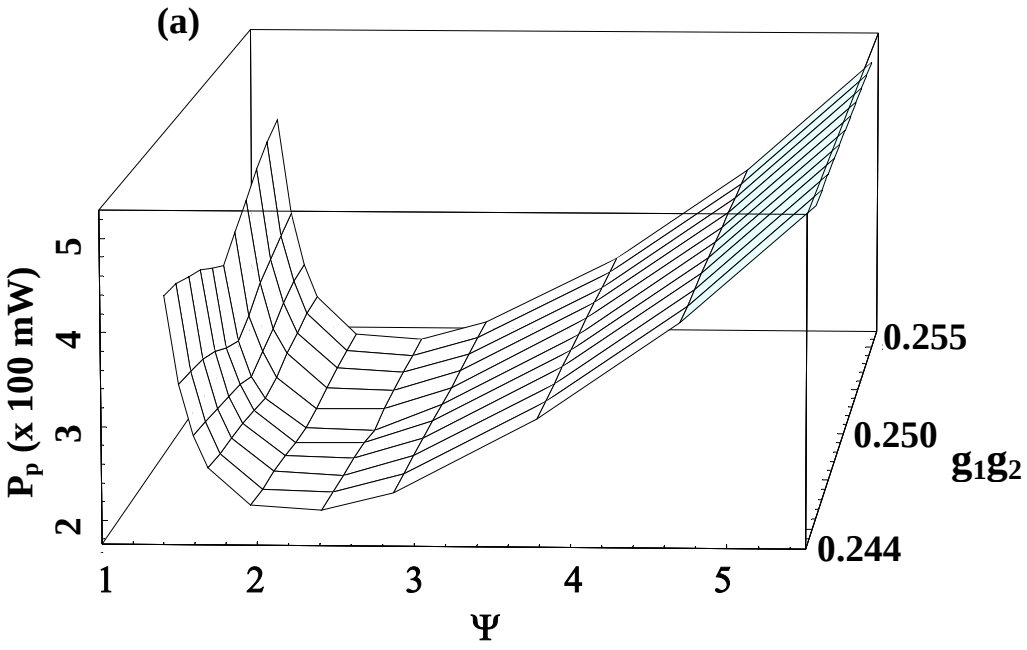

Fig. 2.4. (a) The 3D quasi-periodical bifurcation diagram in terms of P_p, Ψ, and g_1g_2 for $\rho = 0.95$.

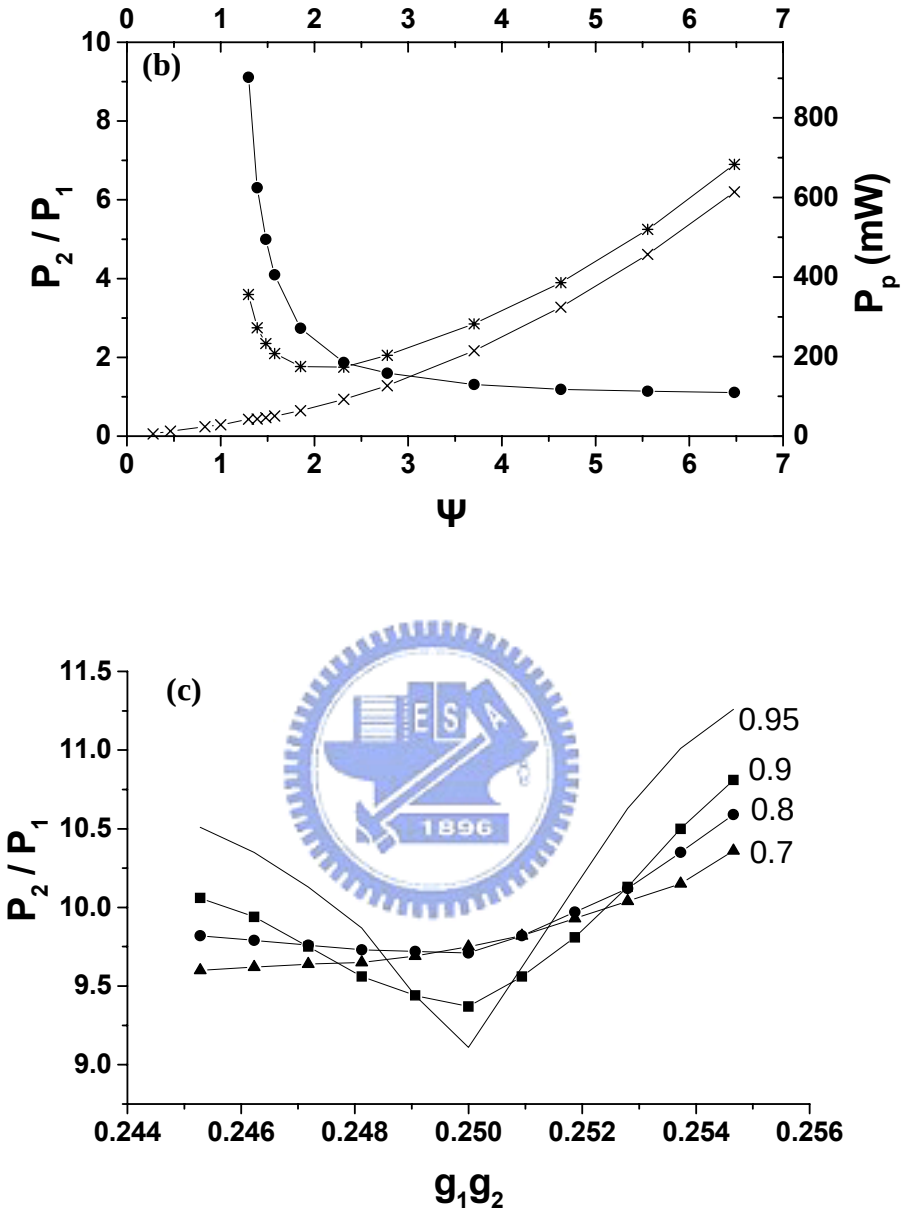

Fig. 2.4. (b) Dependence of the ratio of the instability threshold to the lasing threshold P_2/P_1 on the parameter Ψ for $g_1g_2 = 1/4$ and $\rho = 0.95$. (c) Dependence of on g_1g_2 for $\Psi = 1.3$ with different ρ indicated.

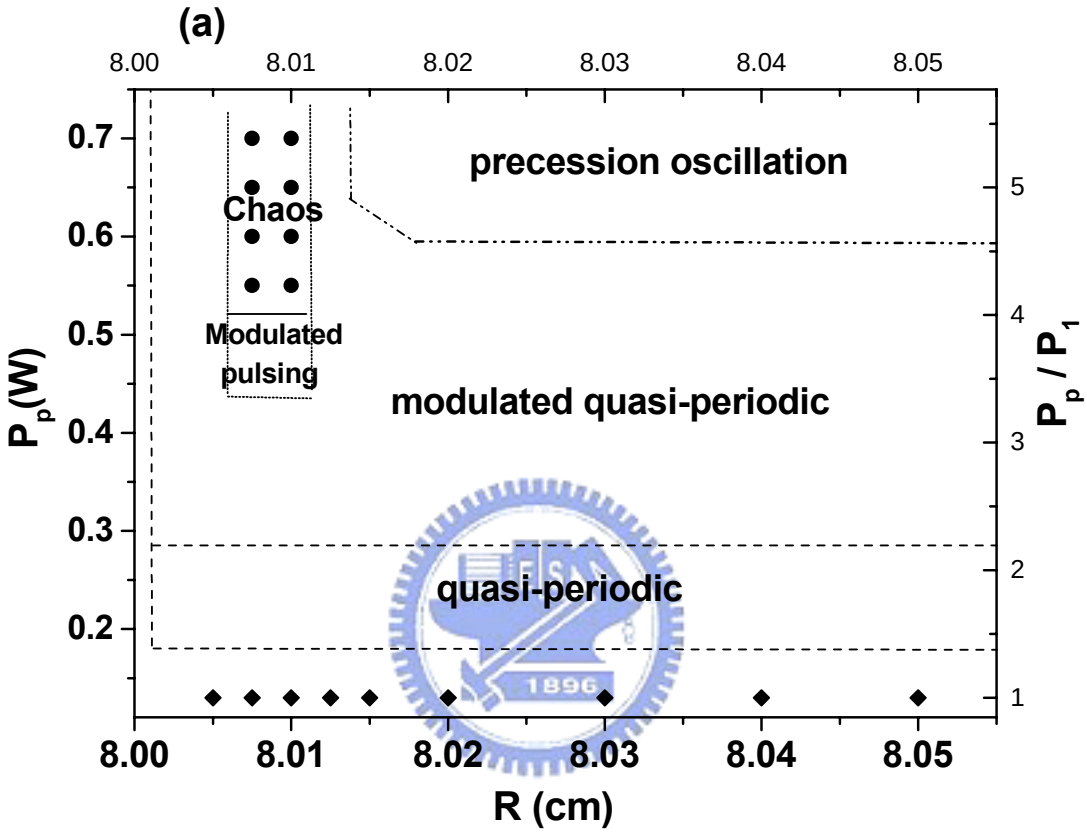

Fig. 2.5. (a) Bifurcation diagram for higher pumping with $\rho = 0.95$ and $\Psi = 2.78$ around $g_1 g_2 = 1/4$.

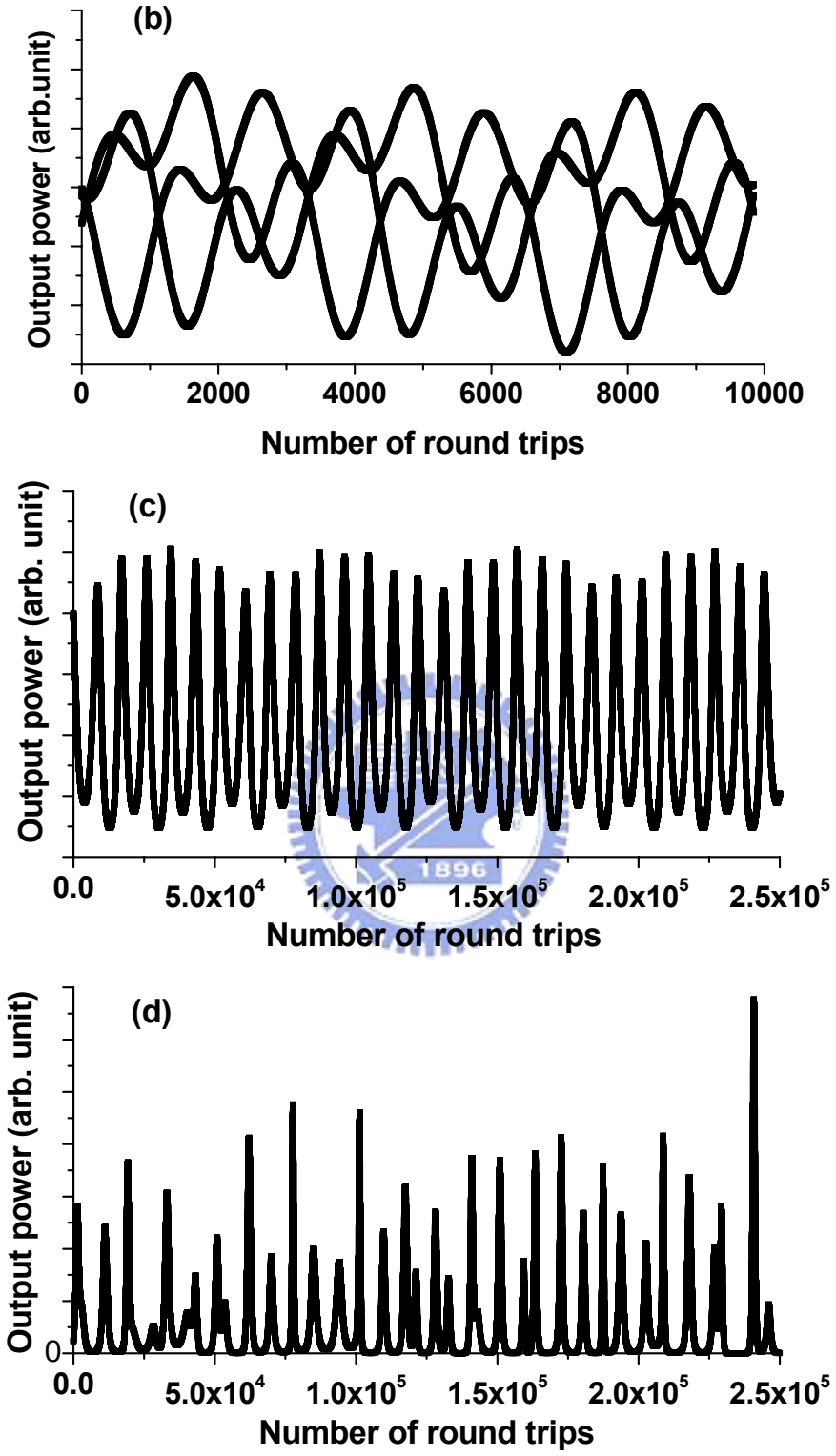

Fig. 2.5. (b)(c)(d) The output power evolution of modulated quasi-period(b), modulated pulsing(c), and chaos(d).

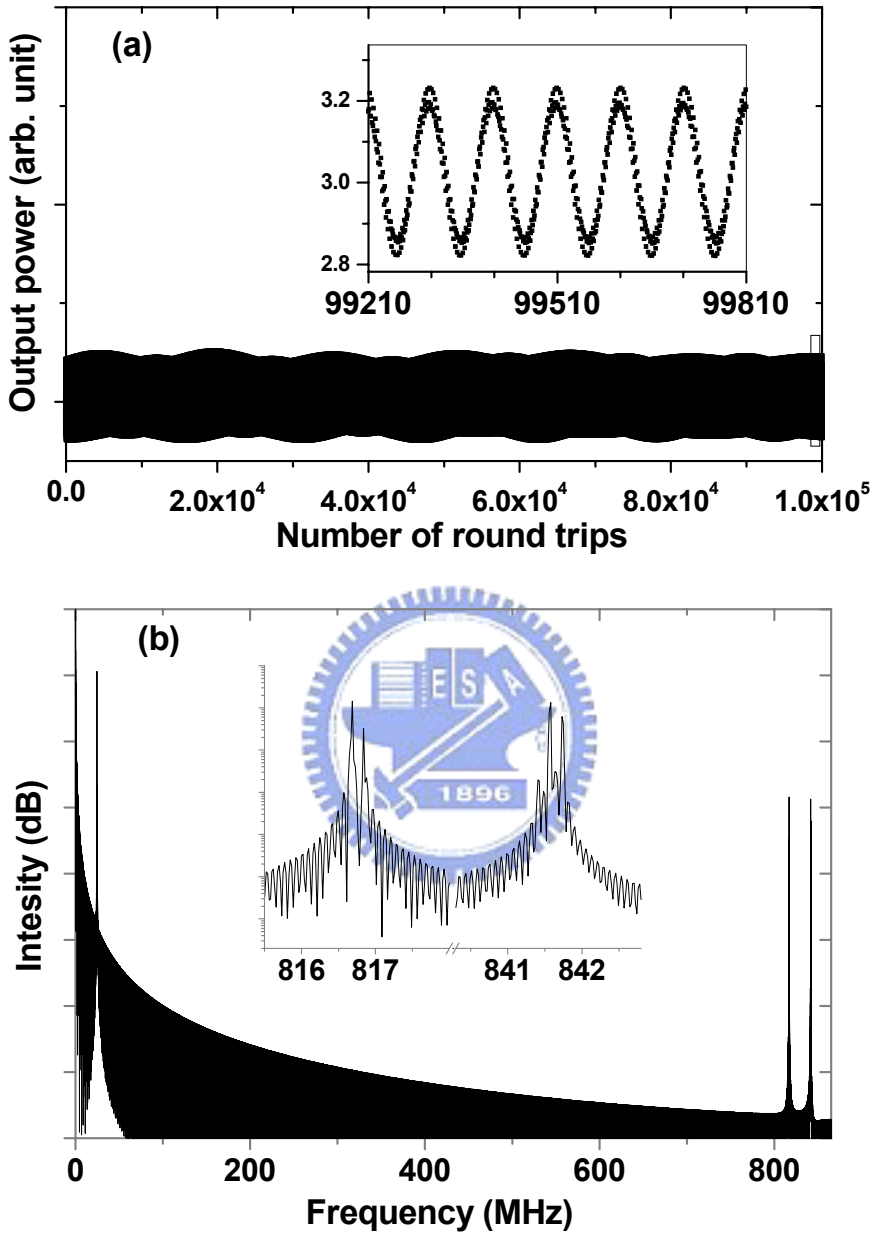

Fig. 2.6. Precession oscillation (a) and power spectrum (b) at g_1g_2 = 0.25466 with ρ = 0.95, Ψ = 2.78, and P_p = 650mW.

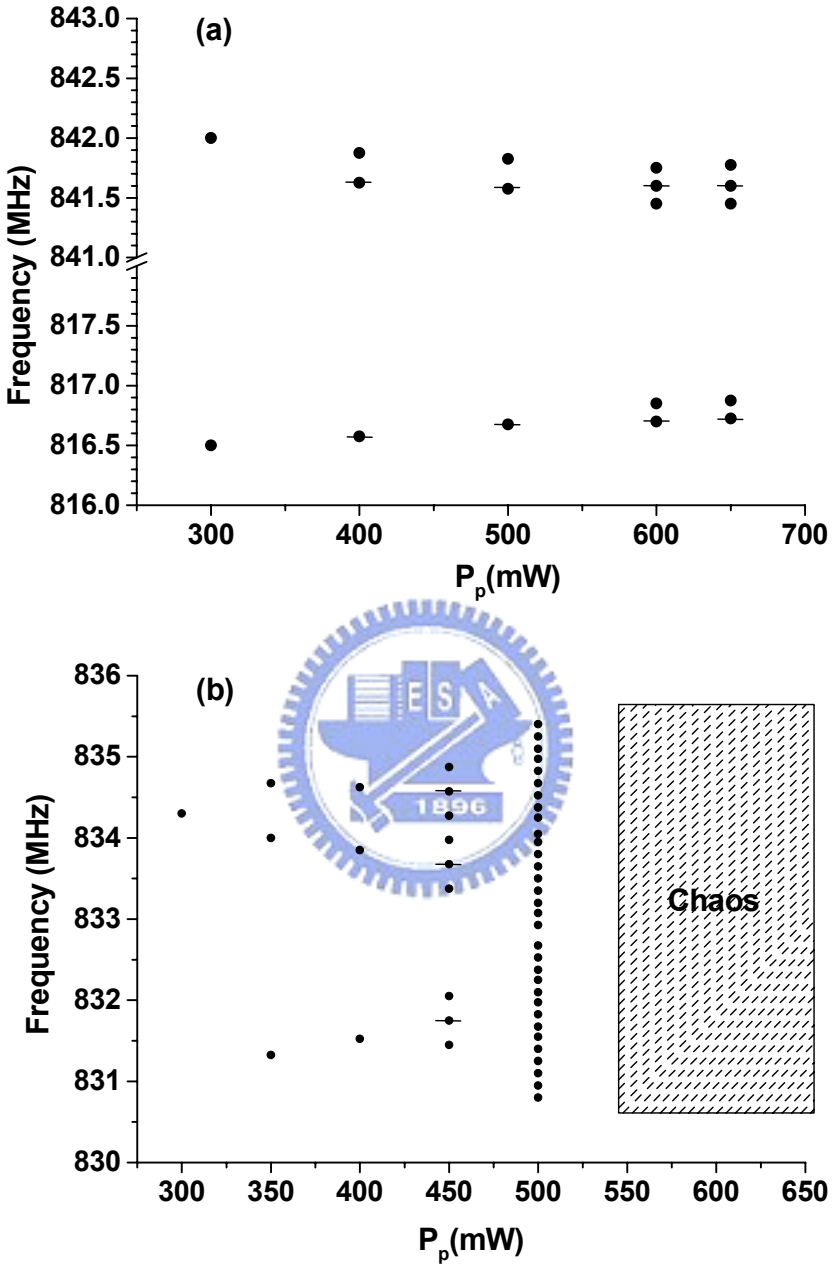

Fig. 2.7. The frequency bifurcation plot using P_p as the parameter for (a) R = 8.05cm and (b) 8.0075cm.

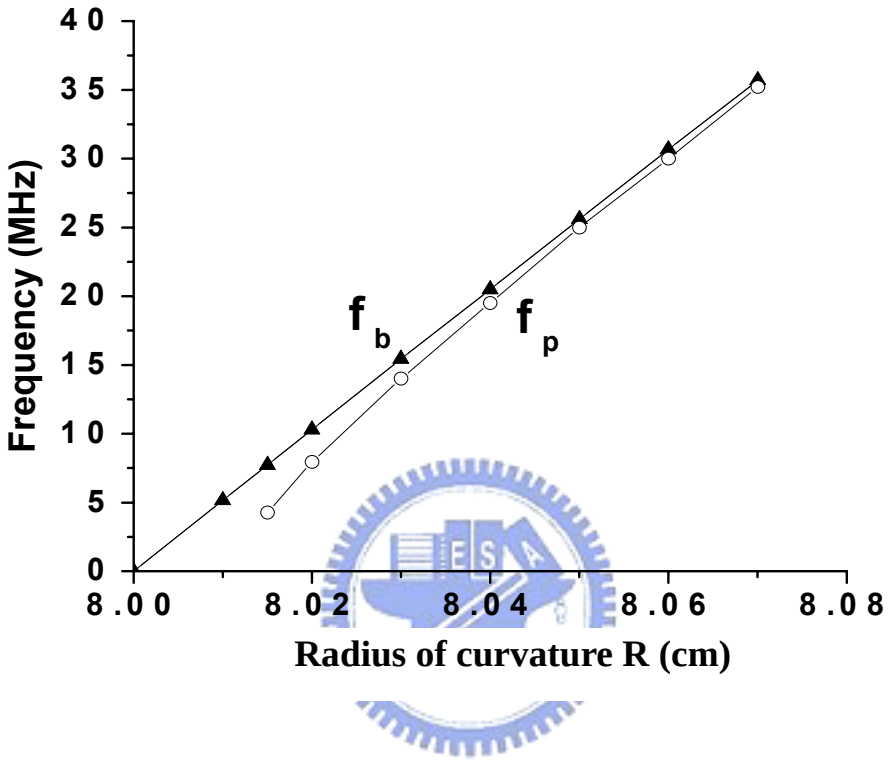

Fig. 2.8. Transverse beat frequency of the cold cavity and the precession frequency versus R for P_p fixed at 650mW.